https://dx.doi.org/10.1016/j.engstruct.2018.02.010

The continuous strength method for the design of high strength steel tubular sections in compression

Xiaoyi Lan[a], Junbo Chen[a], Tak-Ming Chan[a,*], Ben Young[b]

[a] Dept. of Civil and Environmental Engineering, The Hong Kong Polytechnic University, Hung Hom, Hong Kong, China

[b] Dept. of Civil Engineering, The University of Hong Kong, Pokfulam Road, Hong Kong, China

*tak-ming.chan@polyu.edu.hk

Abstract: This paper aims to extend the deformation-based design method named continuous strength method (CSM) for the design of high strength steel tubular sections in compression. The CSM employs a base curve relating the cross-section resistance to its deformation capacity and adopts an elastic, linear hardening material model. Non-slender and slender circular hollow sections (CHS), elliptical hollow sections (EHS), square hollow sections (SHS) and rectangular hollow sections (RHS) were investigated in this study. Hot-finished, cold-formed and built-up steel tubular sections with yield stresses up to 1405 MPa were covered. An extensive numerical study was carried out to supplement the limited test results of high strength steel stub columns in the literature. The cross-section resistances obtained from the proposed CSM, the direct strength method (DSM), and design methods in EN 1993-1-5, EN 1993-1-6, ANSI/AISC 360-10 and AISI S100 were compared with the experimental and numerical capacities of 742 stub columns. It is shown that the proposed CSM can produce more accurate and less scattered strength predictions than the current DSM and design codes.

Keywords: Continuous strength method; Cross-section resistance; High strength steel; Structural design; Tubular sections

1. Introduction

High strength steel (HSS) with a nominal yield stress exceeding 450 MPa has become increasingly popular as an economical and sustainable material. The application of high strength steel can reduce structural self-weight and lower construction costs as well as carbon footprints. Steel tubular sections are widely used due to their aesthetic appearance and advantageous mechanical performance [1]. It is, therefore, imperative to develop design rules for high strength steel tubular sections.

Comprehensive design rules are available for the design of conventional carbon steel cross-sections in design codes and specifications including EN 1993-1-1 [2], EN 1993-1-5 [3], EN 1993-1-6 [4], ANSI/AISC 360-10 [5], AISI S100 [6] and AS/NZS 4600 [7]. The concept of cross-section classification based on the slenderest constituent element within the cross-section and the effective width method are employed for the design of steel cross-section [2, 3, 5-7], and thus the element interaction within the cross-section cannot be taken into account. EN 1993-1-6 [4] adopts shell buckling theory for the design of shells. An elastic, perfectly-plastic material model without considering the beneficial effect of strain hardening is employed in design codes [2-7]. Consequently, the codified design methods without considering the beneficial effects of the element interaction and strain hardening often produce conservative and scattered predictions of cross-section capacity [8-16]. A deformation-based design method called continuous strength method (CSM) was proposed to overcome the inherent drawbacks of the codified design methods [8]. The CSM adopts an elastic, linear hardening material model to exploit the strength enhancement from strain hardening in non-slender steel cross-sections. Furthermore, the CSM

employs a base curve relating deformation capacity of cross-sections to overall cross-section slenderness to consider the element interaction. The CSM has been developed for the design of steel cross-sections using normal strength carbon steel [9-12], stainless steel [12-15] and aluminium alloy [12, 16]. It is shown that the CSM yields more accurate and consistent predictions of cross-section capacity with improved design efficiency compared with the codified design methods.

This study extends the scope of the CSM for the design of non-slender and slender high strength steel tubular sections in compression. Current design methods and the CSM for steel cross-sections in compression were described and compared. Finite element (FE) models were developed and verified against test results in the literature. An extensive parametric study on high strength steel tubular sections was then conducted to supplement the limited test results of high strength steel stub columns in the literature. Non-slender and slender circular hollow sections (CHS), elliptical hollow sections (EHS), square hollow sections (SHS) and rectangular hollow sections (RHS) were investigated. Hot-finished, cold-formed and built-up steel tubular sections were covered. Cross-section resistances collated from experimental tests in the literature and obtained from the numerical study conducted herein were used to assess the current design methods and proposed CSM for high strength steel tubular sections.

2. Current design methods for carbon steel cross-sections

EN 1993-1-5 [3], ANSI/AISC 360-10 [5], AISI S100 [6] and AS/NZS 4600 [7] employ the concept of cross-section classification and the effective width method for the design of normal strength carbon steel cross-sections. Maximum width-to-thickness ratios namely yield slenderness limits are stipulated for compression parts to classify cross-sections into non-slender and slender cross-sections in design codes [2, 3, 5-7]. The yield slenderness limits reflect the influence of steel material properties (yield stress and elastic modulus), edge support conditions (stiffened or unstiffened), and the shape of applied stress field (stress ratio) on the level of susceptibility to local buckling of an element within the cross-section. For cross-sections in compression, cross-sections of Class 1-3 or without slender elements are classified if the width-to-thickness ratio of all constitute elements of the cross-section is within the yield slenderness limit. Otherwise, cross-sections shall be considered as cross-sections of Class 4 or with slender elements. The failure of non-slender cross-sections is normally due to material yielding and/or inelastic local buckling. Thus, the corresponding cross-section resistance can exceed the cross-section yield load which equals to gross cross-sectional area times steel yield stress because of strain hardening. However, an elastic, perfectly-plastic material model without considering the beneficial effect of strain hardening is adopted in design codes [3-7]. Class 4 or slender cross-sections fail before the average stress within the cross-sections reaches steel yield stress due to local buckling.

The nominal strength of Class 1-3 and Class 4 cross-sections in compression specified in EN 1993-1-5 [3] is determined by Eq. (1). EN 1993-1-6 [4] employs shell buckling theory to determine the resistance of shells (e.g. CHS members). The corresponding nominal resistance of shells in compression [4] can be obtained from Eq. (2). The nominal compressive strength of cross-sections subjected to yielding or local buckling in ANSI/AISC 360-10 [5] and AISI S100 [6] can be calculated from Eq. (3) and Eq. (4), respectively.

$$N_{\text{EC3-1-5}} = \begin{cases} f_y A & \text{for } \lambda_1 \le 0.5 + \sqrt{0.085 - 0.055\psi} \\ f_y A_e & \text{for } \lambda_1 > 0.5 + \sqrt{0.085 - 0.055\psi} \end{cases} \qquad \text{(EN 1993-1-5 [3])} \tag{1}$$

$$N_{\text{EC3-1-6}} = \chi f_{\text{y}} A \qquad \text{(EN 1993-1-6 [4])} \qquad (2)$$

$$N_{\text{AISC}} = 0.658^{Qf_{\text{y}}/f_{\text{e}}} Q f_{\text{y}} A \qquad \text{(ANSI/AISC 360-10 [5])} \qquad (3)$$

$$N_{\text{AISI}} = f_{\text{n}} A_{\text{e}} \qquad \text{(AISI S100 [6])} \qquad (4)$$

where A is the gross cross-sectional area, A_{e} is the effective cross-sectional area determined by effective width method, f_{y} is the steel yield stress, λ_{l} is the plate element slenderness, ψ is the stress ratio, χ is the buckling reduction factor determined by the relative slenderness of the shell, Q is the reduction factor related to the effective cross-sectional area and equals to 1.0 for cross-sections without slender elements, f_{e} is the elastic buckling stress specified in Section E3 of ANSI/AISC 360-10 [5], f_{n} is the global column stress determined in accordance with Section E2 of AISI S100 [6]. It is noted that AISI S100 [6] and AS/NZS 4600 [7] adopt the same design equations for cold-formed steel members under compression, and thus the AS/NZS 4600 [7] is not included in the comparison study of Section 8.

The direct strength method (DSM) was proposed by Schafer and Peköz [17, 18] for cold-formed structural steel members with flat elements. The strength-based DSM determines the cross-section capacity as a function of overall cross-section slenderness (λ_{p}) defined by:

$$\lambda_{\text{p}} = \sqrt{f_{\text{y}} / f_{\text{cr}}} \qquad (5)$$

where f_{y} is the steel yield stress and f_{cr} is the elastic buckling stress which may be determined using the bespoken software CUFSM [19], suitable numerical tools such as ABAQUS [20], or approximate equations.

The DSM can consider the beneficial effect of element interaction within the cross-section and improve the design efficiency for slender sections with complex geometries or under stress gradients compared with the effective width method. The DSM is currently incorporated in AISI S100 [6]. The DSM nominal compressive strength of cross-sections subjected to local buckling may be obtained from:

$$N_{\text{DSM}} = \begin{cases} f_{\text{y}} A & \text{for } \lambda_{\text{p}} \le 0.776 \\ (1 - \dfrac{0.15}{\lambda_{\text{p}}^{0.8}}) \dfrac{1}{\lambda_{\text{p}}^{0.8}} f_{\text{y}} A & \text{for } \lambda_{\text{p}} > 0.776 \end{cases} \qquad \text{(Direct Strength Method [6])} \qquad (6)$$

where f_{y} is the steel yield stress, A is the gross cross-sectional area, λ_{p} is the overall cross-section slenderness. It is noted that the DSM also adopts an elastic, perfectly-plastic material model without considering the beneficial effect of strain hardening.

3. The continuous strength method

3.1. General

The continuous strength method (CSM) was originally proposed by Gardner and Nethercot [8] for the design of non-slender cross-sections using stainless steel. The CSM has been developed for the design of cross-sections using normal strength carbon steel, stainless steel and aluminium alloy [8-16]. The base curve relating cross-section deformation capacity to overall cross-section slenderness and the elastic, linear hardening material model are two key components of the CSM. The CSM, therefore, has two major advantages compared with the current design methods, i.e. rational exploitation of strain-hardening and

proper consideration of the element interaction within the cross-section.

3.2. Base curve

The CSM base curve relates the maximum attainable strain (ε_{csm}) to the overall cross-section slenderness (λ_p) as defined by Eq. (5). The base curves proposed for non-slender and slender cross-sections using stainless steel [15] and aluminium alloy [16] in compressions are as follows:

$$\frac{\varepsilon_{csm}}{\varepsilon_y} = \frac{\delta_u / L - 0.002}{\varepsilon_y} = \frac{0.25}{\lambda_p^{3.6}} \le \min(15, \frac{C_1 \varepsilon_u}{\varepsilon_y}) \quad \text{for} \quad \lambda_p \le 0.68 \tag{7}$$

$$\frac{\varepsilon_{csm}}{\varepsilon_y} = \frac{N_u}{N_y} = (1 - \frac{0.222}{\lambda_p^{1.05}}) \frac{1}{\lambda_p^{1.05}} \quad \text{for} \quad \lambda_p > 0.68 \tag{8}$$

where ε_{csm} is the CSM limiting strain, ε_y is the yield strain which equals to f_y/E, f_y is the steel yield stress, E is the steel elastic modulus, ε_u is the ultimate strain at ultimate stress, δ_u is the end shortening at the ultimate load, L is the column length, λ_p is the overall cross-section slenderness, C_1 is the coefficient to define a cut-off strain to avoid over-prediction of material stress, N_u is the ultimate load of stub columns, N_y is the yield load which equals to f_yA. It should be noted that the limiting CSM strain (ε_{csm}) is taken as $\varepsilon_{csm}= \delta_u/L$-0.002 for steel materials with a round material response (e.g. stainless steel, aluminium alloy) and $\varepsilon_{csm}= \delta_u/L$ for those with a sharply defined yield point (e.g. hot-rolled steel) in order to be compatible with the adopted elastic, linear hardening material model [12]. Two upper limits ($15\varepsilon_y$ and $C_1\varepsilon_u$) are stipulated to the CSM limiting strain (ε_{csm}) (see Eq. (7)) to avoid excessive plastic strain and material fracture for non-slender cross-sections. Similarly, Liew and Gardner [10] and Theofanous et al. [11] adopted Eq. (7) to define the base curve for the design of non-slender normal strength carbon steel cross-sections at room and elevated temperatures, respectively. It is noted that the proposed base curve (Eqs. (7-8)) is mainly for the design of SHS and RHS. The base curve proposed by Buchanan et al. [12] for the design of non-slender and slender CHS using stainless steel, aluminium alloy, very high strength carbon steel with yield stresses around 1350 MPa, and normal strength carbon steel is defined as follows:

$$\frac{\varepsilon_{csm}}{\varepsilon_y} = \frac{4.44 \times 10^{-3}}{\lambda_p^{4.5}} \le \min(15, \frac{C_1 \varepsilon_u}{\varepsilon_y}) \quad \text{for} \quad \lambda_p \le 0.3 \tag{9}$$

$$\frac{\varepsilon_{csm}}{\varepsilon_y} = (1 - \frac{0.224}{\lambda_p^{0.342}}) \frac{1}{\lambda_p^{0.342}} \quad \text{for} \quad 0.3 < \lambda_p \le 0.6 \tag{10}$$

3.3. Material models

An elastic, linear strain hardening material model is adopted in the CSM instead of the elastic, perfectly-plastic material model employed in design codes [2-7] and the DSM [17, 18]. The CSM limiting stress (f_{csm}) for steel cross-sections in compression is determined as follows [8-16]:

$$f_{csm} = E\varepsilon_{csm} \quad \text{for} \quad \varepsilon_{csm} / \varepsilon_y < 1.0 \tag{11}$$

$$f_{csm} = f_y + E_{sh}(\varepsilon_{csm} - \varepsilon_y) \quad \text{for} \quad \varepsilon_{csm} / \varepsilon_y \ge 1.0 \tag{12}$$

where E_{sh} is the strain-hardening modulus defined by:

$$E_{sh} = \frac{f_u - f_y}{C_2 \varepsilon_u - \varepsilon_y} \tag{13}$$

where C_2 is the coefficient defining the strain hardening slope, f_u is the ultimate stress, and ε_u is the ultimate strain at ultimate stress which may be obtained from:

$$\varepsilon_u = C_3(1 - f_y / f_u) + C_4 \tag{14}$$

The values of C_1, C_2, C_3 and C_4 proposed by Buchanan et al. [12] are summarized in Table 1.

3.4. Cross-section resistance

The CSM capacity of non-slender and slender cross-sections in compression (N_{csm}) can be determined using Eq. (15) and Eq. (16), respectively [8-16]:

$$N_{csm} = f_{csm} A \tag{15}$$

$$N_{csm} = \left(\varepsilon_{csm} / \varepsilon_y\right) f_y A \tag{16}$$

4. Summary of experimental tests

Results of 277 experimental tests on 115 CHS [21-29], 39 EHS [30-33], and 123 SHS and RHS [21, 25, 26, 34-43] stub columns were collated to assess current design methods and extend the CSM for the design of high strength steel tubular sections. Tables 2-4 show the range of yield stress or 0.2% proof stress (f_y) obtained from coupon tests, the fabrication method of specimens (cold-formed, hot-finished or built-up), the overall cross-section slenderness (λ_p) and the number of tests. The ranges of λ_p in the experimental tests [21-43] are $0.18 \le \lambda_p \le 0.55$ for CHS, $0.23 \le \lambda_p \le 0.51$ for EHS, and $0.23 \le \lambda_p \le 1.71$ for SHS and RHS. A wide range of steel grades with f_y ranging from 216 to 1405 MPa was collated. The majority of CHS, SHS and RHS stub columns in Tables 2 and 4 are made of high strength steel with f_y higher than 450 MPa. Only test results of EHS stub columns using normal strength steel as shown in Table 3 were compiled due to the lack of tests on high strength steel counterparts in the literature. It is noted that experimental tests on CHS, EHS, SHS and RHS stub columns using high strength steel remain limited. Therefore, an extensive numerical investigation as described in Sections 5-6 was conducted to supplement the limited test data.

5. Finite element modelling

5.1. General

Finite element (FE) models have been developed to carry out numerical analysis. The FE simulation in this study was conducted using software ABAQUS [20]. This section describes the FE modelling and validation. Test results of stub columns of CHS [21], EHS [32], and SHS and RHS [21] were used for validation. Tables 5-7 show the parameters of stub columns including the outer diameter of CHS (D), larger outer diameter ($2a$) and smaller outer diameter ($2b$) of EHS, overall section height (H) and overall section width (B) of SHS and RHS, wall thickness (t), maximum imperfection (ω_0), steel yield stress (f_y) of

CHS and EHS, and steel yield stress of flat portions (f_{yf}) and corner regions (f_{yc}) of cold-formed SHS and RHS. Other parameters not listed in Tables 5-7 are detailed in Ma et al. [21] and Chan and Gardner [32]. It should be noted that the residual stress of the stub columns was not modelled in this study due to its insignificant effect on the structural behaviour of stub columns of tubular sections [15, 21]. All degrees of freedom at the two ends of stub columns were restrained except for the axial displacement at one end. The axial load was applied by means of displacement in increments using the "Static" method in ABAQUS. The nonlinear geometric parameter (*NLGEOM) was used to consider the effect of geometric nonlinearity in FE analysis.

5.2. Material properties

The material parameters [21, 32] were adopted including elastic modulus (E), yield stress or 0.2% proof stress (f_y), ultimate stress (f_u), and ultimate strain at ultimate stress (ε_u). The Poisson's ratio (v) of steel materials equals to 0.3. The true stress (σ_T) and logarithmic plastic strain (ε_p) were converted from engineering stress (σ) and engineering strain (ε) [21, 32], and input in FE models according to the recommendation of ABAQUS user's manual [20] as follows:

$$\sigma_T = \sigma(1+\varepsilon) \tag{17}$$

$$\varepsilon_p = \ln(1+\varepsilon) - \sigma_T / E \tag{18}$$

where σ_T and σ are true and engineering stress, respectively, ε_p is logarithmic plastic strain, and ε is engineering strain. It should be noted that the corner portions and extended corner regions up to $2t$ of cold-formed SHS and RHS are strengthened with higher values of f_y due to the cold-forming effect [21]. The effect of cold working was considered by assigning the material properties of the corner regions to the corner portions and extended corner regions. The von Mises yield criterion and isotropic strain hardening rules were used in FE simulation.

5.3. Element type and mesh size

The four-node shell element S4R with reduced integration was adopted. A mesh convergence study was conducted to determine suitable mesh sizes for the stub columns. The mesh sensitivity study shows that the mesh sizes of $D/20$ for CHS, $(2a+2b)/40$ for EHS, and $(H+B)/40$ for SHS and RHS are suitable. The adopted mesh sizes can produce accurate prediction of structural behaviour of the stub columns with reasonable computational costs

5.4. Geometric imperfection

The local geometric imperfection of stub columns was modelled. Elastic eigenvalue analysis was conducted and the obtained lowest elastic buckling mode was used to simulate the distribution of local imperfections. The amplitudes of the lowest buckling mode were taken as the reported maximum local imperfections (ω_0) in Tables 5-7 for the subsequent nonlinear FE simulation.

5.5. Validation

Fig. 1 shows the comparison of typical failure modes of stub columns of CHS, EHS and RHS predicted by FE analysis with those observed in experimental tests [21, 32]. It is shown that the adopted FE models can produce accurate predictions of failure modes of the stub columns. The comparison of load-end shortening curves of representative stub columns [21, 32] is shown in Fig. 2. It is shown that the FE predictions can replicate the load-shortening curves obtained from experimental tests well. Tables 5-7 show the comparison of ultimate loads obtained from FE analysis (N_{FE}) and experimental tests (N_f). The corresponding end-shortenings at ultimate loads obtained from numerical analysis (δ_{FE}) and tests (δ_u) were also compared. It is shown that the predicted loads agree well with the test results with mean values of N_{FE}/N_f equal to unity and maximum coefficient of variation (COV) of 0.04. The predictions of corresponding end-shortening for CHS, SHS and RHS stub columns are reasonably accurate with mean values of δ_{FE}/δ_u close to unity and maximum COV of 0.18, and those for EHS stub columns are relatively scattered. It is noted that repeated tests (e.g. 150×75×4.0-SC1 with δ_u of 0.6 mm and 150×75×4.0-SC2 with δ_u of 1.2 mm) were conducted [32]. Table 6 shows that the test data of end-shortening (δ_u) for almost identical specimens in the repeated tests were scattered. This phenomenon is due to the existence of long yielding plateau in load-shortening curves where the end-shortening varies significantly with almost the same load as shown in Fig. 2 (b). The large variation in the test data of δ_u [32] thus results in the high scatter of δ_{FE}/δ_u for the EHS stub columns (e.g. 150×75×4.0-SC1 with δ_{FE}/δ_u of 2.00 and 150×75×4.0-SC2 with δ_{FE}/δ_u of 0.81).

The validation study shows that the adopted FE models can produce reasonably accurate predictions of failure modes, load-shortening curves, ultimate loads and corresponding end-shortenings of stub columns of CHS, EHS, SHS and RHS. Thus, the validated FE models will be used in the subsequent parametric investigation.

6. Parametric study

The validated FE models were used to conduct an extensive parametric study to supplement limited test results of high strength steel stub columns. A total of 465 high strength steel specimens of CHS, EHS, SHS and RHS were analysed. Table 8 shows the parameters of stub columns including the outer diameter of CHS (D), larger outer diameter ($2a$) and smaller outer diameter ($2b$) of EHS, overall section height (H) and overall section width (B) of SHS and RHS, wall thickness (t), and overall cross-section slenderness (λ_p). The cross-section type is denoted by five letters. The first three letters represent the cross-section shape (CHS, EHS, SHS and RHS) and the last two letters (HF or CF) refer to the fabrication method (hot-finished or cold-formed). The aspect ratio of larger outer diameter ($2a$) to smaller outer diameter ($2b$) of EHS is 2.0. The aspect ratio of overall section height (H) to width (B) of RHS is 1.5 and 2.0. The lengths (L) of stub columns of CHS, EHS, SHS/RHS equal to $3D$, $4a$ and $3H$, respectively. The external radius of SHS and RHS is taken as $1.5t$ for hot-finished specimens, and that of cold-formed specimens equals to $2t$, $2.5t$ and $3t$ for $t \leq 6$, $6 < t \leq 10$ and $10 < t$, respectively, in accordance with EN 10210-2 [44] and EN 10219-2 [45]. It should be noted that the ranges of λ_p in the parametric study are $0.14 \leq \lambda_p \leq 0.76$ for CHS, $0.23 \leq \lambda_p \leq 0.90$ for EHS, and $0.22 \leq \lambda_p \leq 2.61$ for SHS and RHS.

S460, S550 and S690 hot-finished steel, and S700, S900 and S1100 cold-formed steel stub columns of CHS, SHS and RHS were investigated. S460, S550 and S690 hot-finished steel stub columns of EHS were analysed. The values of elastic modulus (E), yield stress (f_y), and ultimate stress (f_u) of S460, S550 and S690 hot-finished steel were taken in accordance with EN 1993-1-1 [2] and EN 1993-1-12 [46], and the ultimate strain at ultimate stress (ε_u) was determined by the predictive equation (see Eq. (28)) proposed by

Yun and Gardner [47]. The bi-linear plus nonlinear hardening material model [47] for hot-finished steel was adopted. The material parameters and stress-strain curves of S700, S900 and S1100 cold-formed steel reported by Ma et al. [48] were employed. Tables 9-10 summarize the adopted material parameters for hot-finished and cold-formed steel stub columns of tubular sections. The corner portions and extended corner regions up to 2t of cold-formed SHS and RHS stub columns were assigned the material properties of corner portions to consider the effect of cold-forming.

The imperfection amplitude (ω_0) of CHS [4] and EHS [49] can be determined as follows:

$$\omega_0 = \frac{t}{Q}\sqrt{\frac{r}{t}} \tag{19}$$

where Q is the fabrication quality parameter taken as 40 (Class A-excellent quality), 25 (Class B-high quality) and 16 (Class C-normal quality), r is the radius of middle surface for CHS and equals to the equivalent radius (i.e. a^2/b) for EHS [49], t is the wall thickness. The maximum out-of-flatness tolerances stipulated in EN 10210-2 [44] and EN 10219-2 [45] are 1.0%H for hot-finished steel SHS and RHS, and 0.8%H with a minimum value of 0.5 mm for cold-formed steel counterparts. It is found that the Class A imperfection for CHS and EHS, and the maximum out-of-flatness tolerances for SHS and RHS are generally the upper bounds to the measured maximum imperfections in experimental tests summarised in Section 4. The upper bounds representing the level of imperfection amplitudes were, therefore, adopted for the parametric study. The boundary condition, element type and mesh size as described in Section 5 were employed. The residual stresses were also not modelled.

7. Extension of the CSM to high strength steel tubular sections

This section extends the continuous strength method (CSM) for the design of high strength steel CHS, EHS, SHS and RHS. The results of experimental tests summarised in Section 4 and numerical study described in Section 6 were used to develop the CSM for the design of non-slender and slender tubular sections using high strength steel.

The limiting overall cross-section slenderness (λ_p) defined by Eq. (5) delineating the transition between non-slender and slender cross-sections was identified by plotting the ultimate load (N_u) normalised by the yield load (N_y=f_yA) of stub columns obtained from tests in the literature and numerical study in Section 6 against the overall cross-section slenderness (λ_p) as shown in Fig. 3. It should be noted that the value of elastic buckling stress (f_{cr}) in this study was determined as follows [12, 49, 50]:

$$f_{cr} = \begin{cases} \dfrac{E}{\sqrt{3(1-\nu^2)}}\dfrac{2t}{D_{eq}} & \text{for CHS and EHS} \\ 4\left(\dfrac{B_1}{H_1}\right)^{1.7}\dfrac{\pi^2 E}{12(1-\nu^2)}\left(\dfrac{t}{B_1}\right)^2 & \text{for SHS and RHS} \end{cases} \tag{20}$$

where E is the elastic modulus, ν is the Poison's ratio which equals to 0.3, t is the wall thickness of tubular sections, D_{eq} is the outer diameter (D) for CHS and the equivalent diameter which equals to $2a^2/b^2$ for EHS, 2a is the outer diameter and 2b is the smaller diameter of EHS, and H_1 is the height and B_1 is the width of the middle surface of SHS and RHS. The limiting CSM strain (ε_{csm}) was taken as ε_{csm}= δ_u/L-0.002 for steel materials with a round material response (e.g. cold-formed high strength steel) and ε_{csm}= δ_u/L for those with a sharply defined yield point (e.g. hot-finished steel). δ_u is the end shortening at the ultimate load obtained from test and numerical investigations, L is the column length, and ε_y is the yield strain which

equals to f_y/E. The weighted average (by area) material properties were adopted for cold-formed tubular sections to consider the strength enhancement in the corners. Fig. 3 shows that the limiting overall cross-section slenderness (λ_p) approximately equals to 0.35 for CHS and EHS, and 0.68 for SHS and RHS, which are generally comparable with the yield slenderness limits proposed by Chan et al. [51] and Zhao et al. [15].

The CSM base curve relates the maximum attainable strain (ε_{csm}) to the overall cross-section slenderness (λ_p). The base curves for non-slender and slender tubular sections using high strength steel were determined by regression analysis to fit the test and numerical data. Fig. 4 shows the proposed base curves defined by Eqs. (21-22) for non-slender and slender CHS and EHS, and the proposed base curves as defined by Eqs. (23-24) for non-slender and slender SHS and RHS are shown in Fig. 5. Two upper limits ($15\varepsilon_y$ and $C_1\varepsilon_u$) are imposed to the CSM limiting strain (ε_{csm}) in Eq. (21) and Eq. (23). The first limit of $15\varepsilon_y$ is to avoid excessive plastic deformation and also corresponds to the material ductility requirement in EN 1993-1-1 [2] and EN 1993-1-12 [46] (i.e. $\varepsilon_u/\varepsilon_y \geq 15$). The second limit of $C_1\varepsilon_u$ which is related to the adopted CSM material models is to avoid over-prediction of ultimate capacity of non-slender steel tubular sections. Upper limits of 0.90 for CHS and EHS, and 2.61 for SHS and RHS are placed upon the base curves for slender tubular sections as numerical and test data have not been examined beyond the upper limits. The base curves for non-slender and slender tubular sections meet at the identified limiting overall cross-section slenderness (i.e. λ_p=0.35 for CHS and EHS, and λ_p=0.68 for SHS and RHS) at a strain ratio ($\varepsilon_{csm}/\varepsilon_y$) of unity.

$$\frac{\varepsilon_{csm}}{\varepsilon_y} = \frac{0.015}{\lambda_p^{4.0}} \leq \min(15, \frac{C_1\varepsilon_u}{\varepsilon_y}) \quad \text{for} \quad \lambda_p \leq 0.35 \tag{21}$$

$$\frac{\varepsilon_{csm}}{\varepsilon_y} = (1 - \frac{0.223}{\lambda_p^{0.44}})\frac{1}{\lambda_p^{0.44}} \quad \text{for} \quad 0.35 < \lambda_p \leq 0.90 \tag{22}$$

$$\frac{\varepsilon_{csm}}{\varepsilon_y} = \frac{0.294}{\lambda_p^{3.174}} \leq \min(15, \frac{C_1\varepsilon_u}{\varepsilon_y}) \quad \text{for} \quad \lambda_p \leq 0.68 \tag{23}$$

$$\frac{\varepsilon_{csm}}{\varepsilon_y} = (1 - \frac{0.219}{\lambda_p^{1.014}})\frac{1}{\lambda_p^{1.014}} \quad \text{for} \quad 0.68 < \lambda_p \leq 2.61 \tag{24}$$

For built-up steel tubular sections with a sharply defined steel yield point and hot-finished steel tubular sections, a quad-linear stress-strain model for hot-rolled steel defined by Eq. (25) [47] was used. The first three stages of the model (i.e. strain up to $C_1\varepsilon_u$) were adopted for the CSM as shown in Fig. 6 to avoid excessive deformation.

$$f_{csm} = \begin{cases} E\varepsilon & \text{for } \varepsilon \leq \varepsilon_y \\ f_y & \text{for } \varepsilon_y < \varepsilon \leq \varepsilon_{sh} \\ f_y + E_{sh}(\varepsilon - \varepsilon_{sh}) & \text{for } \varepsilon_{sh} < \varepsilon \leq C_1\varepsilon_u \\ f_{C_1\varepsilon_u} + \dfrac{f_u - f_{C_1\varepsilon_u}}{\varepsilon_u - C_1\varepsilon_u}(\varepsilon - C_1\varepsilon_u) & \text{for } C_1\varepsilon_u < \varepsilon \leq \varepsilon_u \end{cases} \tag{25}$$

where C_1 is the material coefficient, ε_{sh} is the strain-hardening strain, ε_u is the ultimate strain at ultimate

stress and E_{sh} is the hardening modulus defined as follows:

$$C_1 = \frac{\varepsilon_{sh} + 0.25(\varepsilon_u - \varepsilon_{sh})}{\varepsilon_u} \tag{26}$$

$$\varepsilon_{sh} = 0.1\frac{f_y}{f_u} - 0.055 \quad \text{but } 0.015 \le \varepsilon_{sh} \le 0.03 \tag{27}$$

$$\varepsilon_u = 0.6(1 - \frac{f_y}{f_u}) \quad \text{but } \varepsilon_u \ge 0.06 \tag{28}$$

$$E_{sh} = \frac{f_u - f_y}{0.4(\varepsilon_u - \varepsilon_{sh})} \tag{29}$$

For built-up steel tubular sections with a round material response and cold-formed steel tubular sections, a bi-linear strain hardening material model described in Section 3.3 was adopted as shown in Fig. 7. The values of C_1, C_2, C_3 and C_4 for cold-formed steel listed in Table 1 were employed. The CSM capacity of steel tubular sections in compression (N_{csm}) was determined using Eqs. (15-16).

8. Evaluation of design methods

The proposed CSM and current design methods for high strength steel tubular sections were evaluated. The cross-section resistances obtained from experimental tests in the literature and numerical study in Section 6 (N_u) were compared with the predicted strengths ($N_{u,pred}$) determined in accordance with EN 1993-1-5 [3], EN 1993-1-6 [4], ANSI/AISC 360-10 [5], AISI S100 [6], the DSM [17, 18] and the proposed CSM. All partial factors in design codes were set to unity to allow direct comparison. It is noted that the design method for EHS is not available in current design codes [2-7]. Thus, the cross-section resistance of EHS was obtained from the design equations proposed by McCann et al. [49] ($N_{u,McCann}$), the DSM ($N_{u,DSM}$) and the proposed CSM ($N_{u,CSM}$) for comparison. The measured or modelled geometries and material properties of steel tubular sections were employed. The weighted average (by area) material properties for cold-formed steel tubular sections were adopted. Figs. 8-10 show $N_u/N_{u,pred}$ ratios of CHS, EHS, SHS and RHS stub columns. Tables 11-13 summarise the results of statistical analysis of $N_u/N_{u,pred}$ ratios. The mean values of $N_u/N_{u,pred}$ for CHS obtained from EN 1993-1-6 [4], ANSI/AISC 360-10 [5], AISI S100 [6], the DSM [17, 18] and the proposed CSM are 1.19, 1.18, 1.18, 1.05 and 1.07 with corresponding COV of 0.08, 0.10, 0.10, 0.12 and 0.09. It is shown that the strength predictions from EN 1993-1-6 [4], ANSI/AISC 360-10 [5] and AISI S100 [6] are conservative and consistent, and those from the DSM [17, 18] and the proposed CSM are more accurate and relatively consistent. The mean values of $N_u/N_{u,pred}$ for EHS obtained from McCann et al. [49], the DSM [17, 18] and the proposed CSM are 1.15, 1.02 and 1.06 with corresponding COV of 0.07, 0.11 and 0.08. It is shown that the capacity predictions from McCann et al. [49] are conservative and less scattered, and those from the DSM [17, 18] and the proposed CSM are more accurate and relatively consistent. It should be noted that the mean values of $N_u/N_{u,pred}$ of CHS and EHS are closer to unity for the DSM compared with the proposed CSM. The values of COV of CHS and EHS for the DSM are, however, higher than those of the proposed CSM. This is because the DSM was originally proposed for cold-formed structural steel members with flat plate elements, and the limiting overall cross-section slenderness (λ_p) delineating the transition between non-slender and slender cross-sections

equals to 0.776 in the current DSM (see Eq. (6)). However, such yield slenderness limit adopted by the DSM is not suitable for CHS and EHS as shown in Fig 3(a). The majority of λ_p values for CHS and EHS investigated in this study are lower than 0.776. Therefore, most of CHS and EHS specimens analysed were classified as non-slender cross-sections by the DSM, and the corresponding resistances equal to f_yA as defined by Eq. (6). The DSM generally under-predicts the cross-section strengths of CHS and EHS specimens when $\lambda_p<0.35$ (i.e. the limiting λ_p in the proposed CSM for CHS and EHS), and overestimates the cross-section capacities when $\lambda_p \geq 0.35$, as shown in Figs. 8-9. The mean values of $N_u/N_{u,pred}$ for SHS and RHS obtained from EN 1993-1-5 [3], ANSI/AISC 360-10 [5], AISI S100 [6], the DSM [17, 18] and the proposed CSM are 1.04, 1.02, 1.04, 1.06 and 1.06 with corresponding COV of 0.13, 0.14, 0.13, 0.13 and 0.10. It is shown that the resistance predictions from EN 1993-1-5 [3], ANSI/AISC 360-10 [5], AISI S100 [6] and the DSM [17, 18] are relatively accurate and somewhat scattered, and those from the proposed CSM are accurate and consistent. In general, the proposed CSM can produce more accurate and consistent capacity predictions for the steel tubular sections than the current design codes and the DSM.

The proposed CSM for high strength steel tubular sections can take beneficial effects of strain hardening and element interaction into account. However, it is noted that the ratio of yield stress (f_y) to ultimate stress (f_u) of high strength steel is closer to unity compared with normal strength steel, stainless steel and aluminium alloy. Therefore, the beneficial effect of strain hardening for non-slender tubular sections using high strength steel is less prominent. Furthermore, the application of high strength steel reduces the sizes of structural member and thus the propensity of local buckling of high strength steel members increases. The current codified design methods often require cumbersome calculation for slender cross-sections. The proposed CSM for slender tubular sections using high strength steel provides a simple and accurate design method.

9. Conclusions

The deformation-based design approach termed continuous strength method (CSM) has been extended for the design of non-slender and slender CHS, EHS, SHS and RHS using high strength steel in compression. Hot-finished, cold-formed and built-up steel tubular sections were covered. An extensive numerical study was conducted to supplement the limited test results available in the literature. The proposed CSM, the direct strength method (DSM), and design methods in EN 1993-1-5, EN 1993-1-6, ANSI/AISC 360-10 and AISI S100 were assessed against the experimental and numerical cross-section resistances of 742 stub columns. It is shown that the strength predictions obtained from the proposed CSM are more accurate and consistent than those of the current DSM and design codes.

Acknowledgements

The authors appreciate the support from the Chinese National Engineering Research Centre for Steel Construction (Hong Kong Branch) at the Hong Kong Polytechnic University and the research seed fund from the Hong Kong Polytechnic University (PolyU/1-ZE50). The first author is also grateful for the support given by the Research Grants Council of Hong Kong for the Hong Kong PhD Fellowship Scheme.

References

[1] Wardenier J. Hollow sections in structural applications, 2nd Ed., CIDECT, Geneva; 2011.

400 [2] EN 1993-1-1. Eurocode 3: Design of steel structures – Part 1.1: General rules and rules for buildings.
401 Brussels: European Committee for Standardization (CEN); 2005.
402 [3] EN 1993-1-5. Eurocode 3: Design of steel structures – Part 1.5: Plated structural elements. Brussels:
403 European Committee for Standardization (CEN); 2006.
404 [4] EN 1993-1-6. Eurocode 3: Design of steel structures – Part 1.6: Strength and stability of shell structures.
405 Brussels: European Committee for Standardization (CEN); 2007.
406 [5] ANSI/AISC 360-10. Specification for structural steel buildings. Chicago: American Institute of Steel
407 Construction (AISC); 2010.
408 [6] AISI S100. North American specification for the design of cold-formed steel structural members.
409 Washington: American Iron and Steel Institute (AISI); 2016.
410 [7] AS/NZS 4600. Cold-formed steel structures. Sydney; 2005.
411 [8] Gardner L, Nethercot D. Structural stainless steel design: a new approach. Struct Eng 2004; 82: 2-28.
412 [9] Gardner L. The continuous strength method. Proc ICE – Struct Build 2008;161 (3):127–33.
413 [10] Liew A, Gardner L. Ultimate capacity of structural steel cross-sections under compression, bending
414 and combined loading. Struct 2015; 1:2–11.
415 [11] Theofanous M, Propsert T, Knobloch M, Gardner L. The continuous strength method for steel
416 cross-section design at elevated temperatures. Thin-Walled Struct 2016; 98: 94–102.
417 [12] Buchanan C, Gardner L, Liew A. The continuous strength method for the design of circular hollow
418 sections. J Constr Steel Res 2016; 118:207–16.
419 [13] Afshan S, Gardner L. The continuous strength method for structural stainless steel design.
420 Thin-Walled Struct 2013;68: 42–49.
421 [14] Ahmed S, Ashraf M, Anwar-Us-Saadat M. The continuous strength method for slender stainless steel
422 cross-sections. Thin-Walled Struct 2016; 107: 362–376.
423 [15] Zhao O, Afshan S, Gardner L. Structural response and continuous strength method design of slender
424 stainless steel cross-sections. Eng Struct 2017; 140: 14–25.
425 [16] Su MN, Young B, Gardner L. The continuous strength method for the design of aluminium alloy
426 structural elements. Eng Struct 2016; 122: 338–348.
427 [17] Schafer BW, Peköz T. Direct strength predictions of cold-formed steel members using numerical
428 elastic buckling solutions. In: Proceedings of the fourteenth international speciality conference on
429 cold-formed steel structures. St. Louis (MO, USA); 1998.
430 [18] Schafer BW. Review: the direct strength method of cold-formed steel member design. J Construct
431 Steel Res 2008; 64(7): 766–78.
432 [19] Schafer BW, Ádány S. Buckling analysis of cold-formed steel members using CUFSM: conventional
433 and constrained finite strip methods. In: Proceedings of the eighteenth international speciality
434 conference on cold-formed steel structures. Orlando (USA); 2006.
435 [20] ABAQUS /Standard. Version 6.13-1. USA: K. a. S. Hibbit; 2013.
436 [21] Ma JL, Chan TM, Young B. Experimental investigation on stub-column behavior of cold-formed
437 high-strength steel tubular sections. J Struct Eng 2015; 142(5): 04015174.
438 [22] Ren QX, Han LH, Lam D, Hou C. Experiments on special-shaped CFST stub columns under axial
439 compression. J Construct Steel Res 2014; 98: 123-133.
440 [23] Wei YL, Guo YH, Sun Q, Zhang B. Study on local stability of Q690 high-strength steel tube under
441 axial compression. Chin Civil Eng J 2013; 5: 002. (in Chinese)
442 [24] Giakoumelis G, Lam D. Axial capacity of circular concrete-filled tube columns. J Construct Steel Res
443 2004; 60(7): 1049-1068.

[25] Sakino K, Nakahara H, Morino S, Nishiyama I. Behavior of centrally loaded concrete-filled steel-tube short columns. J Struct Eng 2004; 130(2): 180-188.
[26] Elchalakani M, Zhao XL, Grzebieta R. Tests on concrete filled double-skin (CHS outer and SHS inner) composite short columns under axial compression. Thin-Walled Struct 2002; 40(5): 415-441.
[27] Jiao H, Zhao XL. Imperfection, residual stress and yield slenderness limit of very high strength (VHS) circular steel tubes. J Construct Steel Res 2003; 59(2): 233-249.
[28] Zhao XL. Section capacity of very high strength (VHS) circular tubes under compression. Thin-Walled Struct 2000; 37: 223-40.
[29] Wei S, Mau ST, Vipulanandan C, Mantrala SK. Performance of new sandwich tube under axial loading: experiment. J Struct Eng 1995; 121(12): 1806-1814.
[30] Liu F, Wang Y, Chan, TM. Behaviour of concrete-filled cold-formed elliptical hollow sections with varying aspect ratios. Thin-Walled Struct 2017; 110: 47-61.
[31] Gardner L, Chan TM, Abela JM. Structural behaviour of elliptical hollow sections under combined compression and uniaxial bending. Adv Steel Construct 2011; 7(1): 86-113.
[32] Chan TM, Gardner L. Compressive resistance of hot-rolled elliptical hollow sections. Eng Struct 2008; 30: 522-32.
[33] Gardner L. Structural behaviour of oval hollow sections. Adv Steel Construct 2005; 1(2): 29-53.
[34] Wang J, Afshan S, Schillo N, Theofanous M, Feldmann M, Gardner L. Material properties and compressive local buckling response of high strength steel square and rectangular hollow sections. Eng Struct 2017; 130: 297-315.
[35] Shi G, Zhou W, Bai Y, Lin C. Local buckling of 460MPa high strength steel welded section stub columns under axial compression. J Construct Steel Res 2014; 100: 60-70.
[36] Yoo JH, Kim JW, Yang JG, Kang JW, Lee MJ. Local buckling in the stub columns fabricated with HSA800 of high performance steel. Int J Steel Struct 2013; 13: 445-58.
[37] Gardner L, Saari N, Wang F. Comparative experimental study of hot-rolled and cold-formed rectangular hollow sections. Thin-Walled Struct 2010; 48: 495-507.
[38] Gao L, Sun H, Jin F, Fan H. Load-carrying capacity of high-strength steel box-sections I: Stub columns. J Construct Steel Res 2009; 65: 918-24.
[39] Mursi M, Uy B. Strength of slender concrete filled high strength steel box columns. J Construct Steel Res 2004; 60: 1825-48.
[40] Uy B. Strength of short concrete filled high strength steel box columns. J Construct Steel Res 2001; 57: 113-34.
[41] Rasmussen K, Hancock G. Tests of high strength steel columns. J Construct Steel Res 1995; 34: 27-52.
[42] Usami T, Fukumoto Y. Welded box compression members. J Struct Eng 1984; 110: 2457-70.
[43] Nishino F, Ueda Y, Tall L. Experimental investigation of the buckling of plates with residual stresses. Test Methods for Compression Members. ASTM Int 1967; 419: 12–30.
[44] EN 10210-2. Hot finished structural hollow sections of non-alloy and fine grain steels-Part 2: Tolerances, dimensions and sectional properties. Brussels: European Committee for Standardization (CEN); 2006.
[45] EN 10219-2. Cold formed structural hollow sections of non-alloy and fine grain steels-Part 2: Tolerances, dimensions and sectional properties. Brussels: European Committee for Standardization (CEN); 2006.
[46]EN 1993-1-12. Eurocode 3: Design of steel structures-Part 1-12: additional rules for the extension of

EN 1993 up to steel grades S700, European Committee for Standardization, EN 1993-1-12, CEN. Brussels, 2007.
[47] Yun X, Gardner L. Stress-strain curves for hot-rolled steels. J Construct Steel Res 2017; 133: 36-46.
[48] Ma JL, Chan TM, Young B. Material properties and residual stresses of cold-formed high strength steel hollow sections. J Construct Steel Res 2015; 109: 152-165.
[49] McCann F, Fang C, Gardner L, Silvestre N. Local buckling and ultimate strength of slender elliptical hollow sections in compression. Eng Struct 2016; 111: 104-18.
[50] Seif M, Schafer BW. Local buckling of structural steel shapes. J Construct Steel Res 2010; 66(10): 1232-1247.
[51] Chan TM, Zhao XL, Young B. Cross-section classification for cold-formed and built-up high strength carbon and stainless steel tubes under compression. J Construct Steel Res 2015; 106: 289-295.

Table 1

Coefficients for the CSM bi-linear material models (Buchanan et al. [12]).

Steel type	C_1	C_2	C_3	C_4
Very high strength steel	0.40	0.45	0.60	0
Cold-formed steel	0.40	0.45	0.60	0
Austenitic and duplex stainless steel	0.10	0.16	1.00	0
Ferritic stainless steel	0.40	0.45	0.60	0
Aluminium	0.50	0.50	0.13	0.06

Table 2

Experimental tests on CHS stub columns.

Reference	f_y (MPa)	Fabrication method	λ_p	No. of tests
Ma et al. [21]	1014-1180	Cold-formed	0.31-0.40	9
Ren et al. [22]	389	Cold-formed	0.30	2
Wei et al. [23]	740	Cold-formed	0.27-0.48	24
Giakoumelis and Lam [24]	343, 365	Hot-finished	0.18, 0.20	2
Sakino et al. [25]	283-835	Cold-formed	0.23-0.43	9
Elchalakani et al. [26]	357-454	Cold-formed	0.20-0.30	8
Jiao and Zhao [27]	433-1398	Cold-formed	0.21-0.52	10
Zhao [28]	1341-1405	Cold-formed	0.30-0.37	12
Wei et al. [29]	216-524	Cold-formed	0.23-0.55	39
Total				115

Table 3

Experimental tests on EHS stub columns.

Reference	f_y (MPa)	Fabrication method	λ_p	No. of tests
Liu et al. [30]	376	Cold-formed	0.51	3
Gardner et al. [31]	365-410	Hot-finished	0.26-0.30	4
Chan and Gardner [32]	364-434	Hot-finished	0.23-0.43	25
Gardner [33]	378-414	Hot-finished	0.23-0.35	7
Total				39

Table 4

Experimental tests on SHS and RHS stub columns.

Reference	f_y (MPa)	Fabrication method	λ_p	No. of tests
Wang et al. [34]	498-799	Hot-finished	0.23-0.66	11
	531-1234	Cold-formed	0.78-1.54	18
Ma et al. [21]	663-1187	Cold-formed	0.63-1.23	16
Shi et al. [35]	493-532	Built-up	0.46-1.65	4
Yoo et al. [36]	761	Built-up	0.30-0.95	5
Gardner et al. [37]	361-534	Cold-formed	0.24-0.70	10
	449-504	Hot-finished	0.24-0.59	10
Gao et al. [38]	793	Built-up	0.60-1.71	4
Sakino et al. [25]	262-835	Cold-formed	0.38-1.40	21
Mursi and Uy [39]	761	Built-up	0.67-1.62	4
Elchalakani et al. [26]	392-598	Cold-formed	0.57-0.62	3
Uy [40]	784	Built-up	0.68	2
Rasmussen and Hancock [41]	705	Built-up	0.52	1
Usami and Fukumoto [42]	568	Built-up	0.81-1.62	6
Nishino et al. [43]	266-800	Built-up	0.77-1.40	8
Total				123

Table 5

Comparison of numerical results with test data of CHS stub columns [21].

Specimen	D (mm)	t (mm)	ω_0 (mm)	f_y (MPa)	δ_u (mm)	N_f (kN)	δ_{FE}/δ_u	N_{FE}/N_f
V89×3-S	89.0	2.96	0.174	1054	3.79	886	0.82	1.02
V89×3-S#	89.0	2.94	0.174	1054	3.83	898	0.81	1.00
V89×4-S	89.0	3.89	0.133	1053	5.01	1171	0.74	1.00
S89×4-S	88.9	3.91	0.072	1180	5.08	1375	0.72	0.98
S89×4-S#	89.1	3.92	0.116	1180	4.94	1365	0.75	0.99
S108×4-S	108.2	3.90	0.141	1180	4.81	1671	0.91	0.99
S133×4-S	133.4	3.91	0.174	1159	5.34	2018	0.96	1.01
S133×4-S#	133.7	3.93	0.173	1159	5.99	1985	0.85	1.03
S139×6-S	139.5	5.92	0.168	1014	7.71	3344	0.86	0.99
Mean							0.82	1.00
COV							0.10	0.01

Table 6

Comparison of numerical results with test data of EHS stub columns [32].

Specimen	$2a$ (mm)	$2b$ (mm)	t (mm)	ω_0 (mm)	f_y (MPa)	δ_u (mm)	N_f (kN)	δ_{FE}/δ_u	N_{FE}/N_f
150×75×4.0-SC1	150.44	75.60	4.18	0.04	380	0.6	538	2.00	1.05
150×75×4.0-SC2	150.47	75.40	4.22	0.07	373	1.2	554	0.81	1.01
150×75×5.0-SC1	150.17	75.80	5.08	0.05	374	0.7	689	1.80	0.98
150×75×5.0-SC2	150.19	75.68	5.14	0.08	364	2.5	700	1.48	0.95
150×75×6.3-SC1	148.66	75.98	6.27	0.04	381	9.5	896	1.20	1.05
150×75×6.3-SC2	148.77	75.95	6.28	0.06	400	11.6	935	0.75	1.00
150×75×6.3-SC3	149.83	74.87	6.52	0.07	406	13.7	931	0.61	1.03
150×75×6.3-SC4	150.24	75.16	6.34	0.05	415	10.5	952	0.89	1.05
150×75×8.0-SC1	150.11	75.10	8.66	1.75	369	18.2	1367	0.73	0.97
150×75×8.0-SC2	149.17	75.07	8.51	0.12	386	18.8	1435	0.95	1.01
400×200×8.0-SC1	395.73	207.36	7.63	0.78	434	1.5	2961	1.00	1.04
400×200×10.0-SC1	394.55	209.49	9.60	0.82	380	2.4	3521	0.78	1.00
400×200×12.5-SC1	402.20	200.41	12.01	0.49	373	2.4	4727	2.53	0.94
400×200×14.0-SC1	400.51	199.47	14.42	0.45	374	18.7	5610	0.87	0.95
400×200×16.0-SC1	403.45	201.18	15.35	0.15	364	14.8	6310	1.15	1.00
500×250×8.0-SC1	492.35	261.20	7.59	0.75	381	2.5	3684	0.78	0.98
Mean								1.15	1.00
COV								0.47	0.04

Table 7

Comparison of numerical results with test data of SHS and RHS stub columns [21].

Specimen	H (mm)	B (mm)	t (mm)	ω_0 (mm)	f_{yf} (MPa)	f_{yc} (MPa)	δ_u (mm)	N_f (kN)	δ_{FE}/δ_u	N_{FE}/N_f
H80×80×4-S	80.4	80.1	3.94	0.172	792	933	3.12	1016	0.64	0.99
H100×100×4-S	100.5	100.2	3.92	0.253	735	931	1.94	1157	0.84	0.98
H120×120×4-S	120.9	120.7	3.92	0.162	689	923	1.48	1160	1.01	1.04
H140×140×5-S	140.2	141.0	4.94	0.280	708	912	2.45	1974	0.86	0.95
H140×140×6-S	141.1	141.1	5.96	0.230	663	859	3.99	2456	0.80	1.02
H160×160×4-S	160.5	160.3	3.97	0.654	744	910	2.45	1206	0.86	1.01
H100×50×4-S	100.2	50.5	3.94	0.251	724	859	2.35	875	0.94	1.00
H200×120×5-S	200.3	120.5	4.94	0.420	738	895	2.23	1776	1.23	1.05
V80×80×4-S	80.4	80.2	3.94	0.214	1005	1187	2.92	1363	0.66	0.97
V100×100×4-S	100.3	100.4	3.97	0.284	978	1114	2.09	1401	0.87	1.00
V120×120×4-S	121.2	121.4	3.92	0.394	960	1114	1.91	1375	0.90	0.96
Mean									0.92	1.00
COV									0.18	0.03

Table 8

Parameters of hot-finished and cold-formed high strength steel stub columns of CHS, EHS, SHS and RHS.

Cross-section	D (mm)	$2a \times 2b$ (mm)	$H \times B$ (mm)	t (mm)	λ_p
CHS-HF	101.6	-	-	1, 2, 3.2, 5, 10	0.14-0.59
	219.1	-	-	2, 4, 5, 10, 16	
	323.9	-	-	3, 4, 5, 10, 16	
	406.4	-	-	4, 6, 8, 12.5, 16	
	508.0	-	-	4, 6, 8, 12.5, 16	
CHS-CF	101.6	-	-	1, 2, 3.2, 5, 10	0.17-0.76
	219.1	-	-	2, 4, 5, 10, 16	
	323.9	-	-	3, 4, 5, 10, 16	
	406.4	-	-	4, 6, 8, 12.5, 16	
	508.0	-	-	4, 6, 8, 12.5, 16	
EHS-HF	-	150×75	-	1, 2, 4, 6.3, 10	0.23-0.90
	-	200×100	-	2, 4, 6.3, 8, 12.5	
	-	250×123	-	3, 4, 6, 10, 12.5	
	-	300×150	-	3, 4, 8, 12.5, 16	
	-	400×200	-	4, 6, 8, 12, 14	
SHS-HF	-	-	100×100	1.5, 2, 4, 6.3, 10	0.22-2.23
	-	-	200×200	3, 4, 5, 10, 16	
	-	-	300×300	4, 5, 6.3, 10, 16	
	-	-	400×400	6, 8, 10, 14.2, 16	
SHS-CF	-	-	100×100	1.6, 3, 5, 6, 8	0.38-2.61
	-	-	200×200	2.9, 5, 8, 12, 15	
	-	-	300×300	4.5, 6, 8, 12, 20	
	-	-	400×400	7, 9, 10, 12, 16	
RHS-HF	-	-	150×100	2.5, 3, 4, 6.3, 10	0.35-1.95
	-	-	200×100	2.9, 3.5, 4, 8, 10	
	-	-	300×200	4.5, 5, 5.5, 10, 16	
	-	-	400×200	5.5, 6.3, 10, 14.2, 16	
RHS-CF	-	-	150×100	4, 6, 8, 9.4, 10	0.43-2.35
	-	-	200×100	3.4, 3.8, 4.1, 8.8, 9.4	
	-	-	300×200	6, 6.4, 7.5, 15, 17.6	
	-	-	400×200	5.8, 6, 6.4, 11, 14	

Table 9

Material parameters for hot-finished high strength steel stub columns of CHS, EHS, SHS and RHS.

Steel grade	E (GPa)	f_y (MPa)	f_u (MPa)	ε_u (%)
S460	210	460	550	9.82
S550	210	550	640	8.44
S690	210	690	770	6.23

Table 10

Material parameters for cold-formed high strength steel stub columns of CHS, SHS and RHS (Ma et al. [48]).

Steel grade	CHS				Flat portion of SHS and RHS				Corner portion of SHS and RHS			
	E (GPa)	f_y (MPa)	f_u (MPa)	ε_u (%)	E (GPa)	f_y (MPa)	f_u (MPa)	ε_u (%)	E (GPa)	f_y (MPa)	f_u (MPa)	ε_u (%)
S700	214	772	816	4.64	212	719	840	4.28	212	897	983	1.63
S900	210	1054	1116	2.26	208	982	1149	2.08	209	1138	1245	2.17
S1100	207	1152	1317	2.20	205	1073	1356	2.03	206	1245	1470	2.12

Table 11

Statistical analysis for 265 CHS stub columns.

	N_u / $N_{u,EC3\text{-}1\text{-}6}$	N_u / $N_{u,AISC}$	N_u / $N_{u,AISI}$	N_u / $N_{u,DSM}$	N_u / $N_{u,CSM}$
Mean	1.19	1.18	1.18	1.05	1.07
COV	0.08	0.10	0.10	0.12	0.09

Table 12

Statistical analysis for 114 EHS stub columns.

	$N_u / N_{u,McCann}$	$N_u / N_{u,DSM}$	$N_u / N_{u,CSM}$
Mean	1.15	1.02	1.06
COV	0.07	0.11	0.08

Table 13

Statistical analysis for 363 SHS and RHS stub columns.

	N_u / $N_{u,EC3\text{-}1\text{-}5}$	N_u / $N_{u,AISC}$	N_u / $N_{u,AISI}$	N_u / $N_{u,DSM}$	N_u / $N_{u,CSM}$
Mean	1.04	1.02	1.04	1.06	1.06
COV	0.13	0.14	0.13	0.13	0.10

(a) S133×4-S [21]

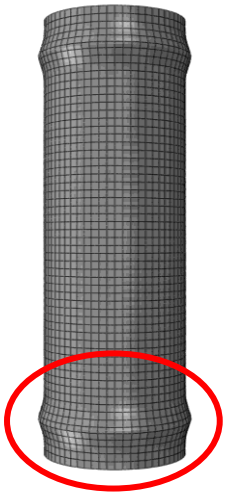

(b) FEA-CHS

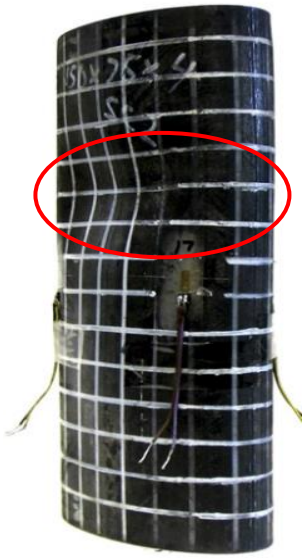

(c) 150×75×4 SC1 [32]

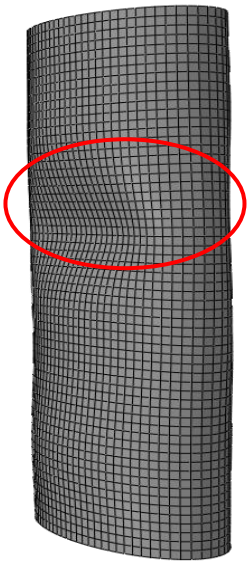

(d) FEA-EHS

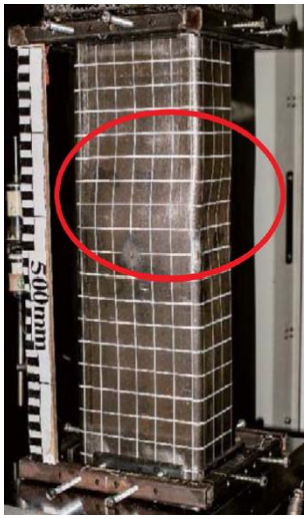

(e) H160×160×4-S [21]

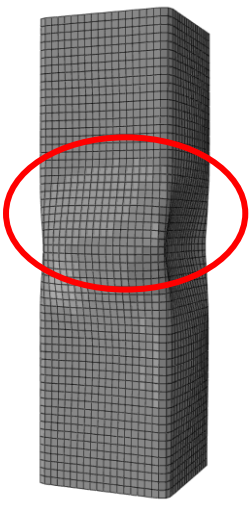

(f) FEA-SHS

Fig. 1. Comparison of failure modes observed in tests with those predicted by FE analysis.

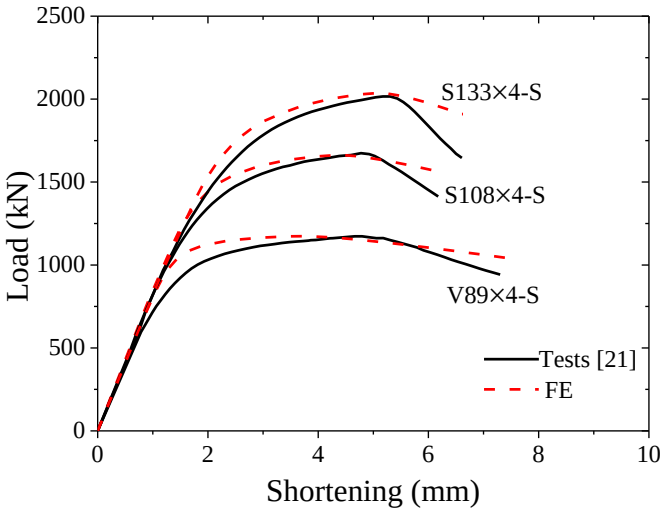

(a) CHS

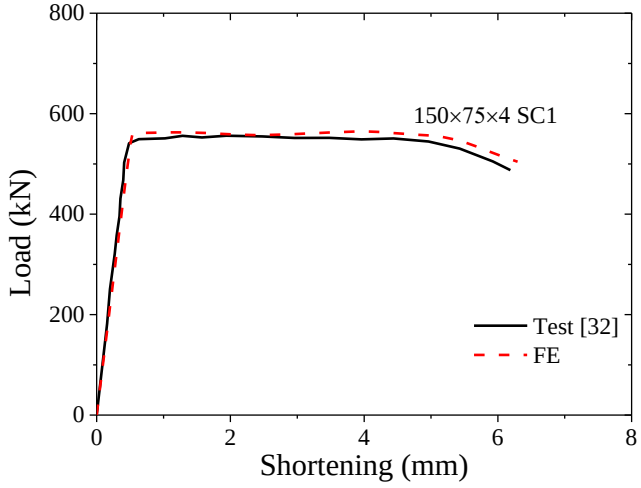

(b) EHS

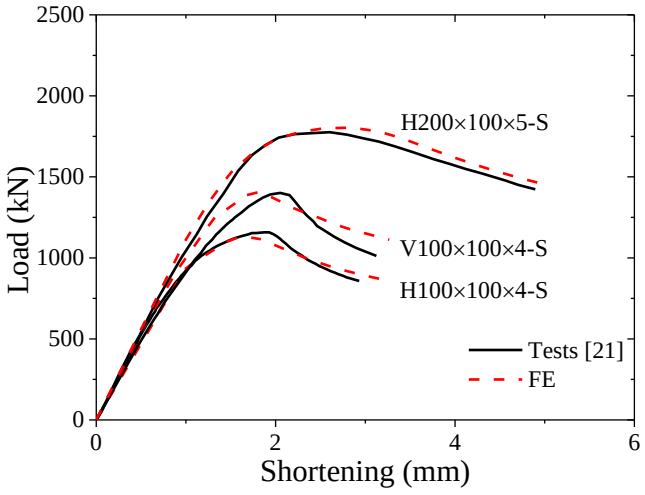

(c) SHS and RHS

Fig. 2. Comparison of load-shortening curves.

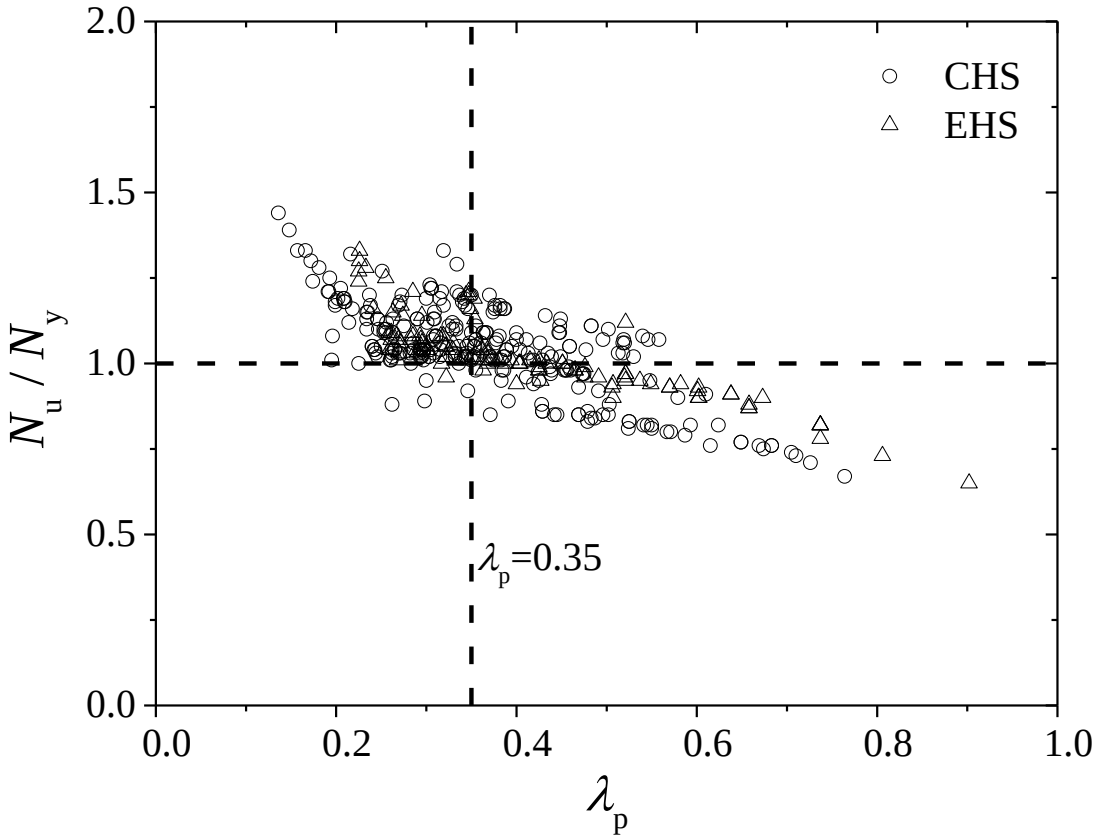

(a) CHS and EHS

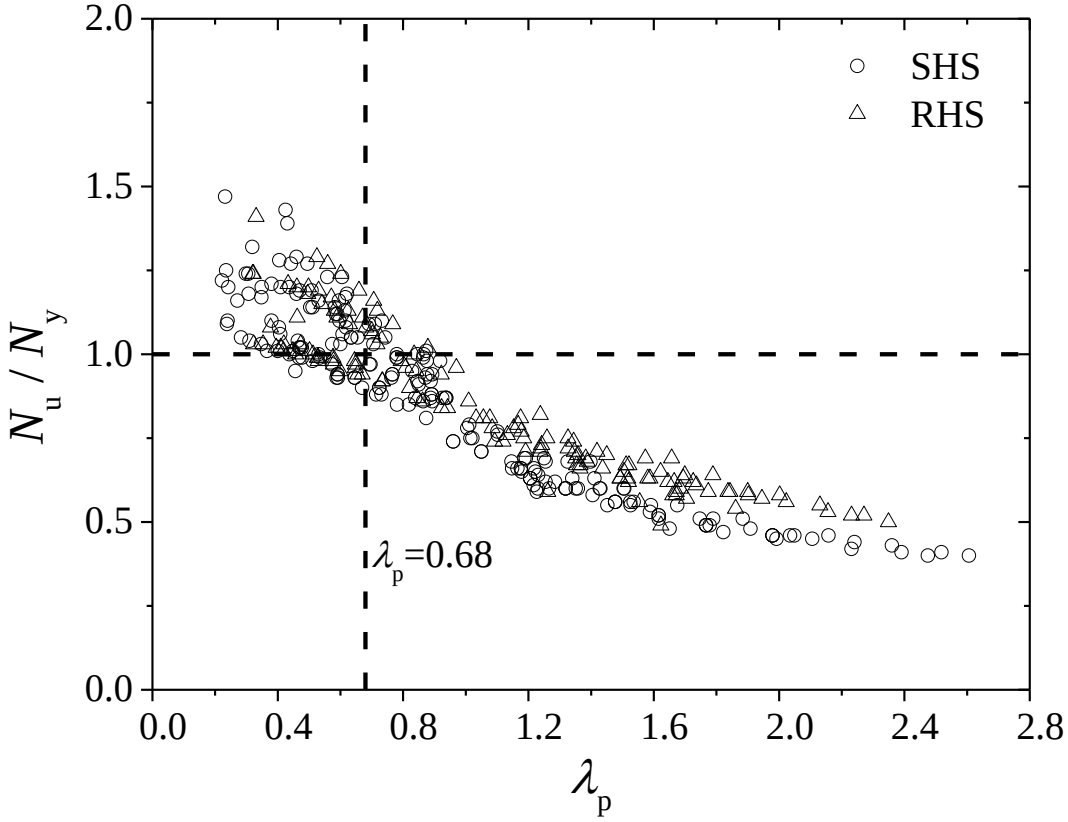

(b) SHS and RHS

Fig. 3. Ultimate load normalised by yield load of stub columns.

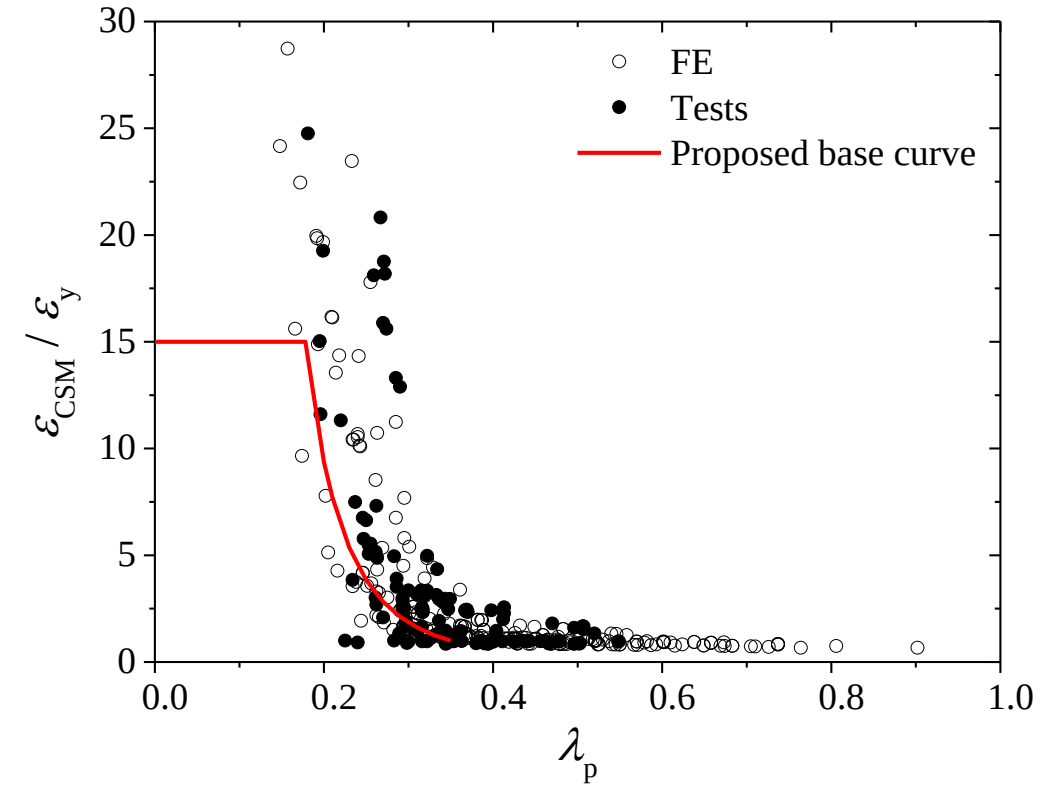

(a) Non-slender cross-sections

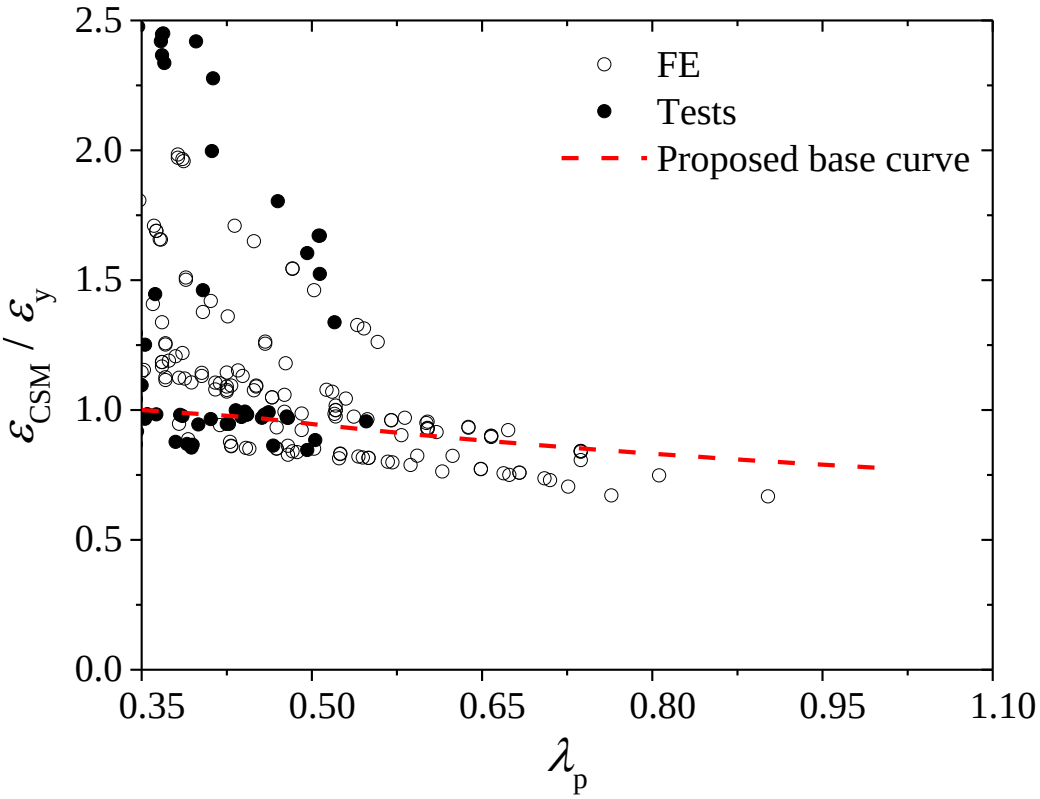

(b) Slender cross-sections

Fig. 4. Base curves for CHS and EHS with test and numerical data.

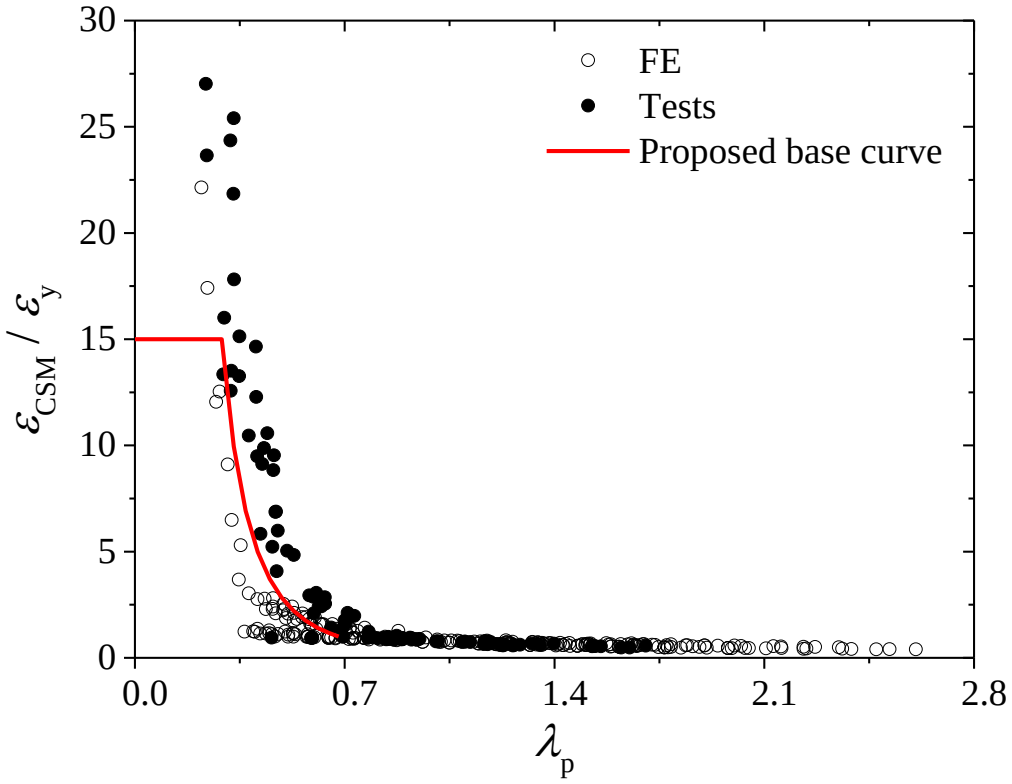

(a) Non-slender cross-sections

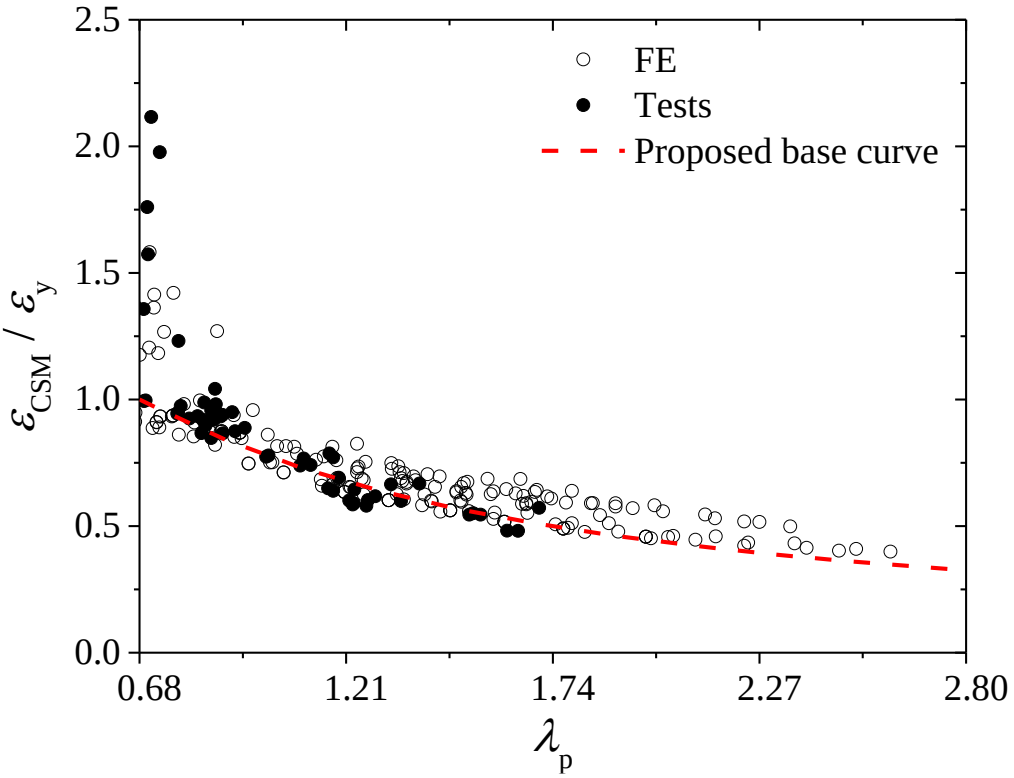

(b) Slender cross-sections

Fig. 5. Base curves for SHS and RHS with test and numerical data.

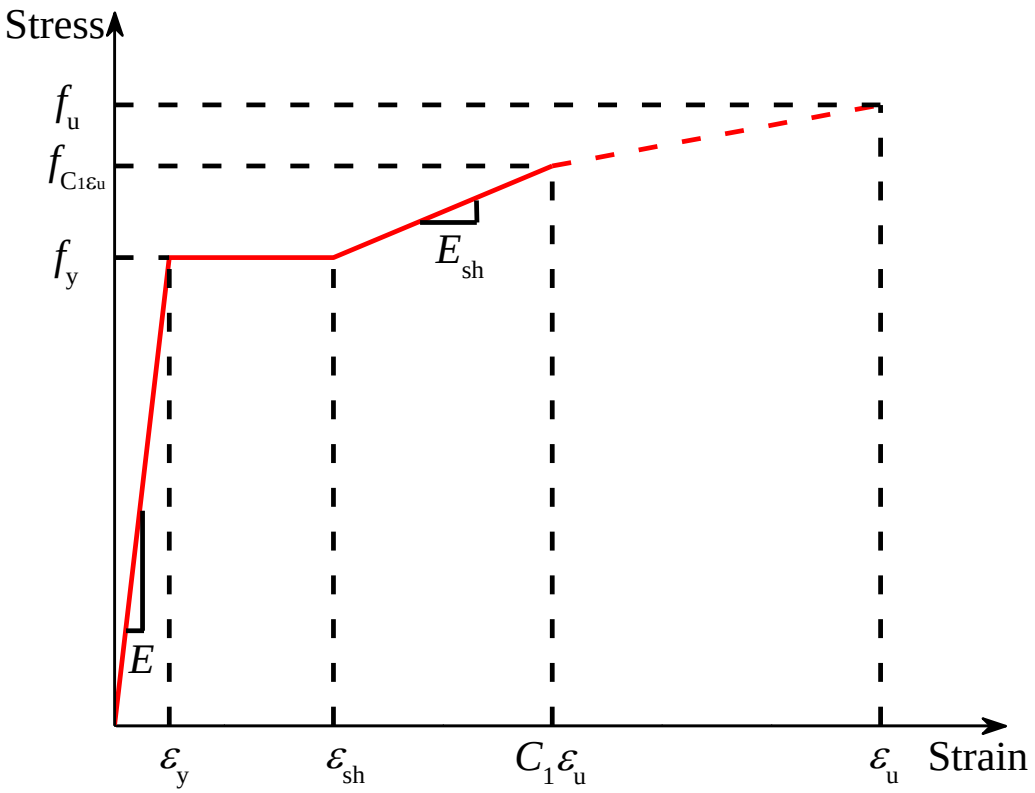

Fig. 6. CSM tri-linear material model.

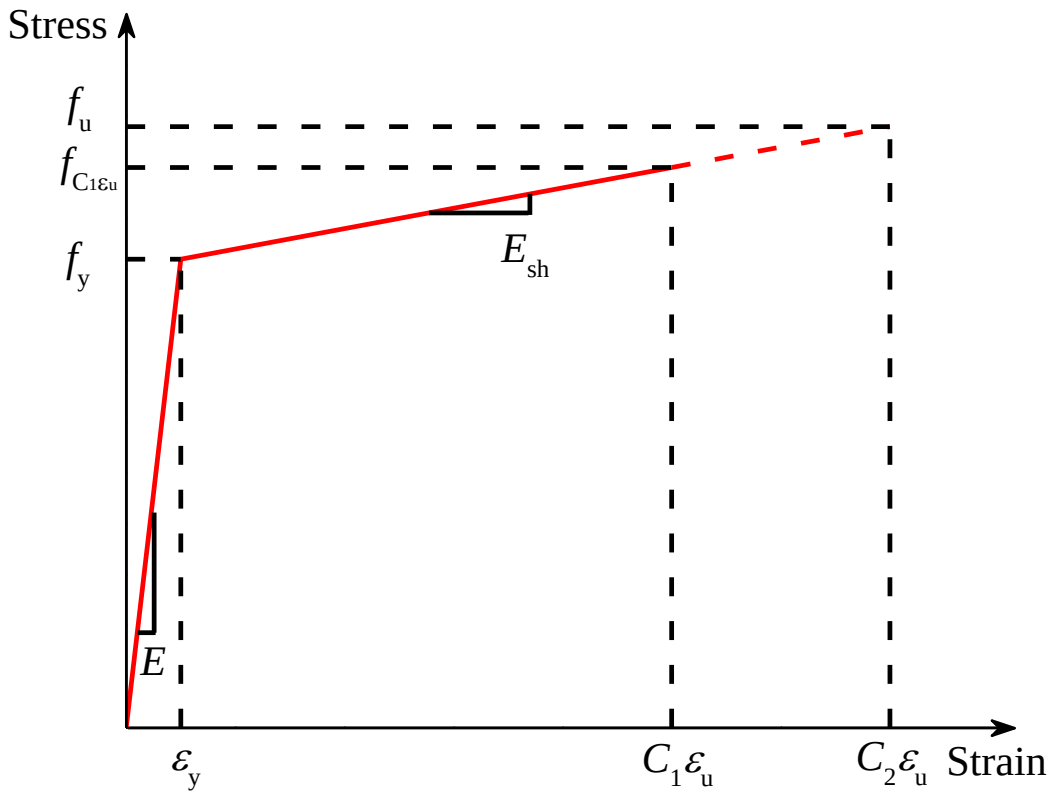

Fig. 7. CSM bi-linear material model.

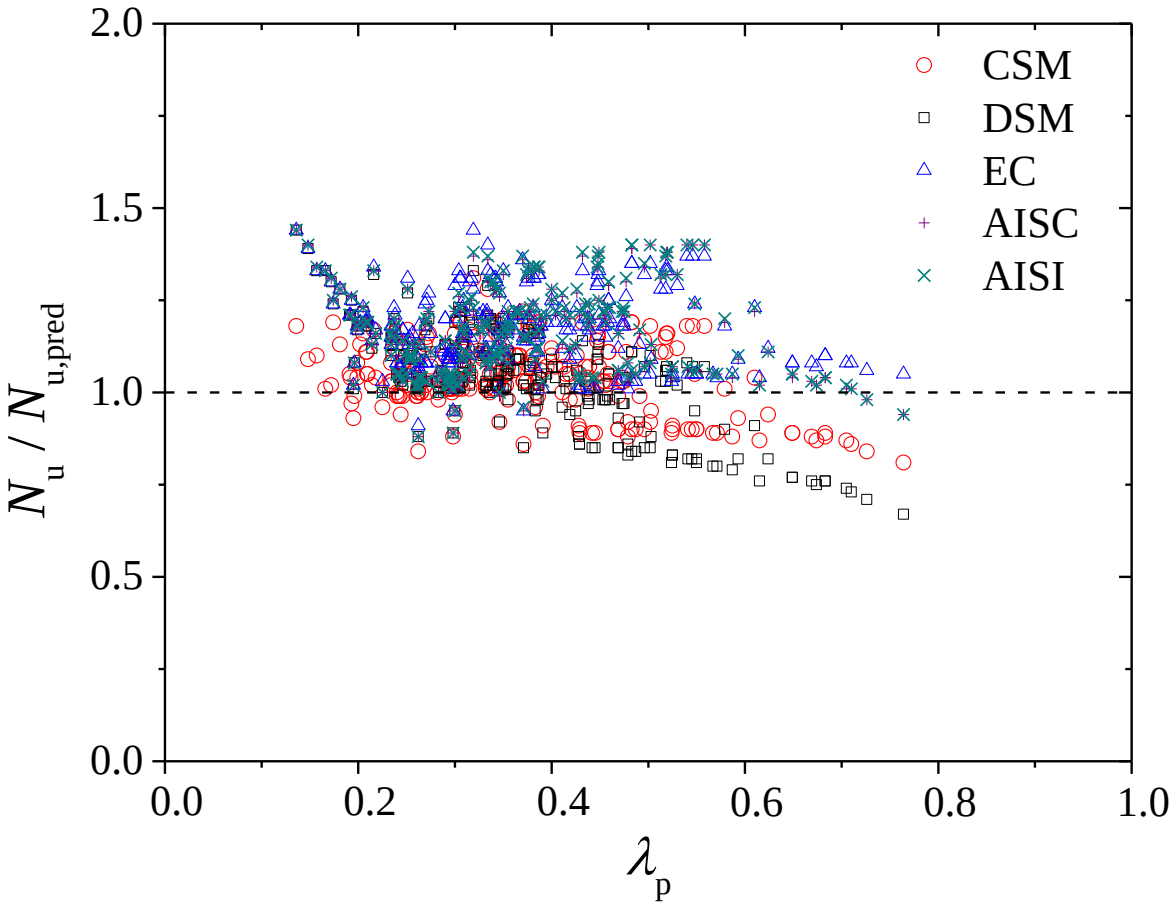

Fig. 8. Comparison of test and numerical capacities of 265 CHS stub columns with predicted strengths.

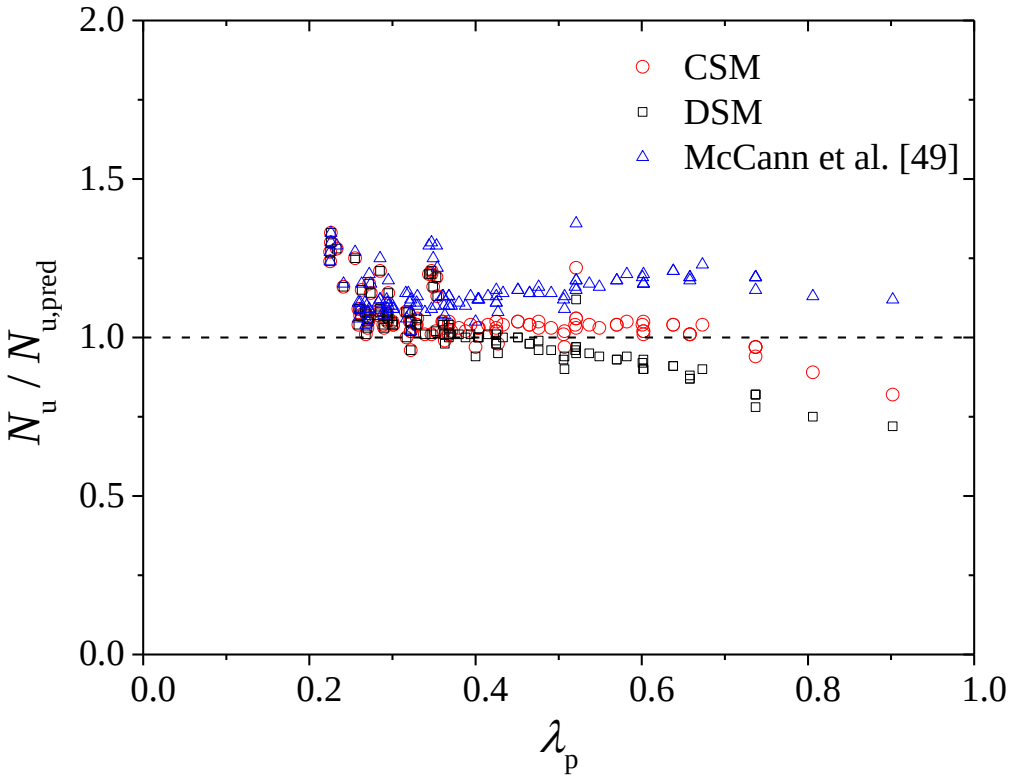

Fig. 9. Comparison of test and numerical capacities of 114 EHS stub columns with predicted strengths.

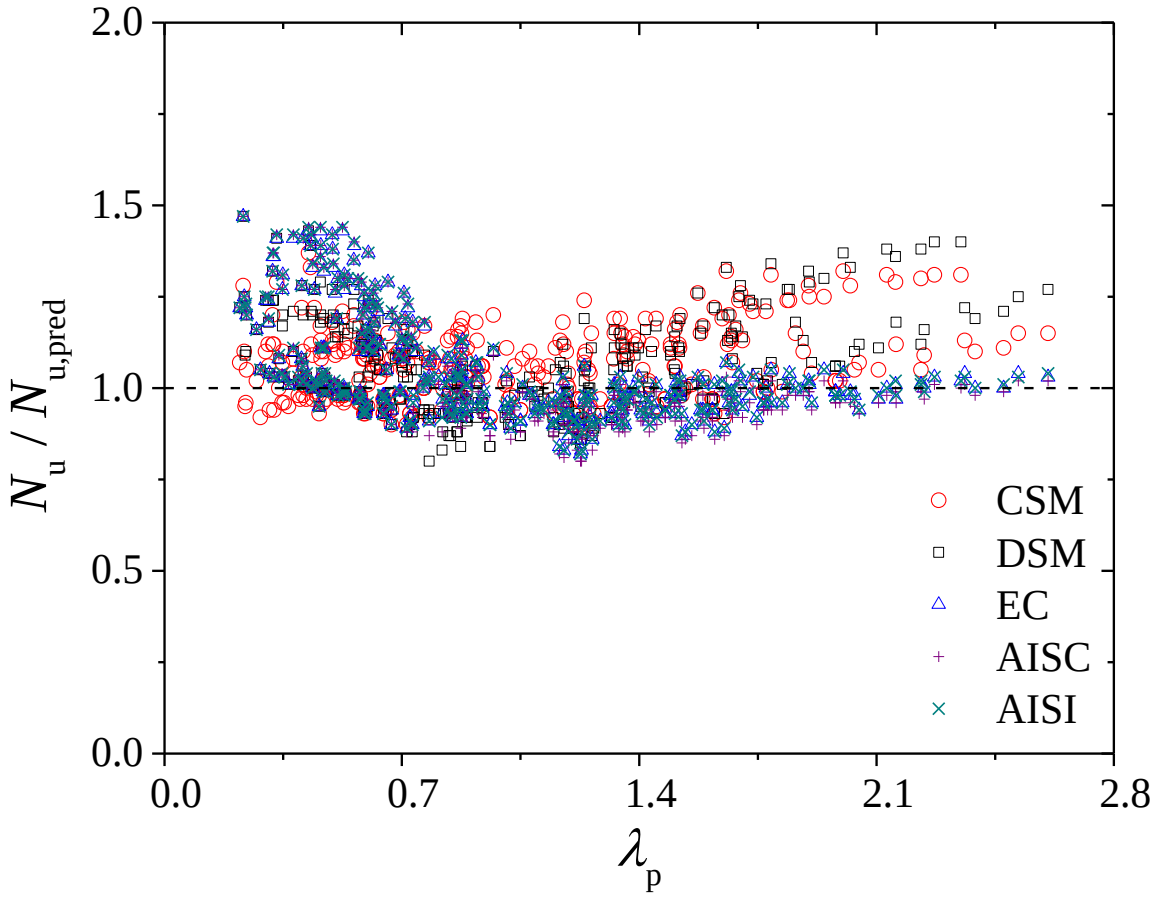

Fig. 10. Comparison of test and numerical capacities of 363 SHS and RHS stub columns with predicted strengths.